Chiral structures and tunable magnetic moments in 3d transition metal doped Pt_6 clusters*

Zhang Xiu-Rong(张秀荣)[a)†], Yang Xing(杨 星)[b)], and Ding Xun-Lei(丁迅雷)[c)]

[a)] *School of Mathematics and Physics, Jiangsu University of Science and Technology, Zhenjiang* 212003, *China*

[b)] *School of Materials Science and Engineering, Jiangsu University of Science and Technology, Zhenjiang* 212003, *China*

[c)] *Beijing National Laboratory for Molecular Sciences (BNLMS), State Key Laboratory for Structural Chemistry of Unstable and Stable Species, Institute of Chemistry, Chinese Academy of Sciences, Beijing* 100190, *China*

(Received 2 February 2012; revised manuscript received 31 March 2012)

The structural, electronic, and magnetic properties of transition metal doped platinum clusters $M\mathrm{Pt}_6$ (M=Sc, Ti, V, Cr, Mn, Fe, Co, Ni, Cu, and Zn) are systematically studied by using the relativistic all-electron density functional theory with the generalized gradient approximation. Most of the doped clusters show larger binding energies than the pure Pt_7 cluster, which indicates that the doping of the transition metal atom can stabilize the pure platinum cluster. The results of highest occupied molecular orbital (HOMO)–lowest unoccupied molecular orbital (LUMO) gaps suggest that the doped clusters can have higher chemical activities than the pure Pt_7 cluster. The magnetism calculations demonstrate that the variation range of the magnetic moments of the $M\mathrm{Pt}_6$ clusters is from 0 μ_B to 7 μ_B, revealing that the $M\mathrm{Pt}_6$ clusters have the potential utility in designing new spintronic nanomaterials with tunable magnetic properties.

Keywords: alloy clusters, chiral structure, stability, magnetic property

PACS: 36.40.Cg, 61.46.–w, 71.15.Mb **DOI:** 10.1088/1674-1056/21/9/093601

1. Introduction

Recently, platinum (Pt) nanoparticles have aroused considerable interest due to their unique physical and chemical properties, particularly, their superior catalytic activities for a number of reactions.[1,2] Pt is one of the noble metals, the high cost hampers its application and commercialization as a perfect catalyst in practice. Alloying Pt with some relatively small base metals has the advantages of reducing the amount of Pt used and improving the activity and stability at the same time as compared with the pure Pt catalyst.[3] It has been demonstrated that when Pt is alloyed with transition metals (TM), such as Cr, Mn, Fe, Co, and Ni, a two- to four-fold improvement in oxygen reduction reaction (ORR) specific activity compared with the Pt catalyst can be achieved.[4−10] Stamenkovic *et al.*[11] studied polycrystalline alloy films of Pt_3M catalysts (M=Ni, Co, Fe, and Ti) to understand the role of transition metals in the electrocatalytic ORR activity of Pt alloys. They found that in these Pt_3M alloys, the first outer layer was enriched by Pt due to the surface segregation. This Pt over layer structure was found to be fairly stable in 0.1 M HClO_4 solution, and the catalytic activity for the ORR was dependent on the nature of the transition metal. The Pt alloys with Ni, Co, and Fe were much more active than the pure Pt, while the Pt alloys with the earlier transition metals exhibited less enhancement. Nørskov *et al.*[12] studied nanoscale effects on the electro catalytic activity using density functional theory (DFT) calculations and showed that the alloys of Pt with Ni, Co, Fe, and Cr (where Pt was segregated on the surface) had smaller oxygen binding energies than the pure Pt. Their results provided good explanations for the experimental observations that the Pt skins on these alloys had higher catalytic activities than the pure Pt. Yang *et al.*[13] have prepared the carbon supported Pt-metal nanoparticles with diameters of about 5–20 nm by using a chemical impregnation method. The hydrolytic activities of Pt-alloy catalysts were in the order of PtRu > Pt_3Au > PtIr > PtCo > Pt_3Ni > PtCu > PtSn∼Pt in the sense of hydrogen generation rate and yield. Antolini

*Project supported by the National Natural Science Foundation of China (Grant No. 51072072) and the Jiangsu Provincial Natural Science Foundation, China (Grant No. BK2010343).

†Corresponding author. E-mail: zh4403701@126.com

© 2012 Chinese Physical Society and IOP Publishing Ltd

et al.[14] investigated the relationship between the stability of the second metal and its content in the alloy using $Pt_{1-x}M_x$ (M=Fe, Co, and Ni), and revealed that when x was small, only the unalloyed base metal could be dissolved. However, if x was increased to 0.6, even an alloyed metal could be dissolved from the bulk alloy. Xiong and Manthiram[15,16] claimed that alloys with ordered structures might further enhance the catalytic activity by optimizing several factors, including (i) the geometric and the electronic structures of Pt with the optimum number of base metal atoms as nearest neighbors, (ii) the d-electron density in the Pt atomic surface configuration, and (iii) the Pt–Pt distance.

Although many experimental and theoretical studies concentrate on strategies for developing nanostructured Pt alloys as electro catalysts for ORR, there is no clear answer about the dominant factors in the catalyst activity enhancement. Since the extent to which such nanostructured Pt alloys enhance the catalyst activity and stability is strongly dependent on the geometric and the electronic effects, the research on the geometric structures and the electronic properties of transition-metal doped platinum clusters using DFT is indispensable. Moreover, there have been some experimental and theoretical researches on mixed metal clusters, dealing with the structural and the magnetic properties of clusters for better magnetic material design.[17,18] For ascertaining the structure/property evolution of pure platinum clusters growing from a small size to a large size and ultimately to the bulk[19] and the special size Pt_7 cluster studied in Ref. [20], in the present paper, we carry out systematic first-principles investigation of the structural, electronic, and magnetic properties of the Pt_6 clusters doped with transition metals, MPt_6 (M=Sc, Ti, V, Cr, Mn, Fe, Co, Ni, Cu, and Zn).

2. Computational details

The electronic structures and the magnetic properties of MPt_6 (M=Sc, Ti, V, Cr, Mn, Fe, Co, Ni, Cu, and Zn) are calculated using the DFT method[21,22] implemented in the DMol^3 package.[23] The electron density functional is treated by the generalized gradient approximation (GGA) with the PW91 exchange–correlation functional parametrized by Perdew and Wang.[24] All-electron spin-unrestricted calculations with scalar relativity (via VPSR tag) and double-numerical basis set including d polarization functions (DND)[25] are employed in this work. The Mulliken population analysis is perform to obtain the net spin populations on each atom. In the geometry optimization, the convergence thresholds are set to be 0.002 Hartree/Å for the force and 0.005 Å for the displacement. The global orbital cutoff quality is set to be fine to describe the electronic wave functions. Self-consistent field calculations are done with a convergence criterion of 1×10^{-5} Hartree on the total energy without thermal smearing of the orbital occupation. There are no imaginary frequencies for all the structures reported here, indicating that they are minima on the potential energy surface. In addition, for the geometry optimization of each isomer, the spin multiplicity is considered at least to be 1, 3, 5, 7, and 9 for even-electron clusters ($TiPt_6$, $CrPt_6$, $FePt_6$, $NiPt_6$, and $ZnPt_6$) and 2, 4, 6, 8, and 10 for odd-electron clusters ($ScPt_6$, VPt_6, $MnPt_6$, $CoPt_6$, and $CuPt_6$). If the total energy decreases with the spin multiplicity increasing, we will consider higher spin states until the energy minimum with respect to the spin multiplicity is reached.

Benchmark calculations are performed on the Pt_2 cluster. The calculated bond length, vibrational frequency, and binding energy of the Pt_2 cluster are 2.347 Å, 239.7 cm^{-1}, and 3.34 eV, respectively, which are in excellent agreement with the available experiment data (2.333 Å, 222.5 cm^{-1}, and 3.14 eV).[26–28] Test calculations are also performed for the $NiPt_6$ cluster at the B3LYP/LANL2DZ level with the Gaussian 03 package. The ground-state structure found in this work is a metastable structure, but is only 0.154 eV higher in energy than the ground-state structure, which indicates that the method used in this work is quite reliable.

3. Results and discussion

3.1. Geometrical structure

To find the lowest-energy structures of bimetallic MPt_6 (M = Sc, Ti, V, Cr, Mn, Fe, Co, Ni, Cu, and Zn) clusters and the Pt_7 cluster, we consider a large number of initial configurations, which are constructed based on the intuitions and the stable structures of pure Pt_n clusters with capping, substitution, or padding M atoms. Various stable isomers are found for Pt_7 and MPt_6 clusters, and the typical structures (structures (a)–(j)) are summarized in Fig. 1, and the corresponding energetic and structural parameters are given in Table 1.

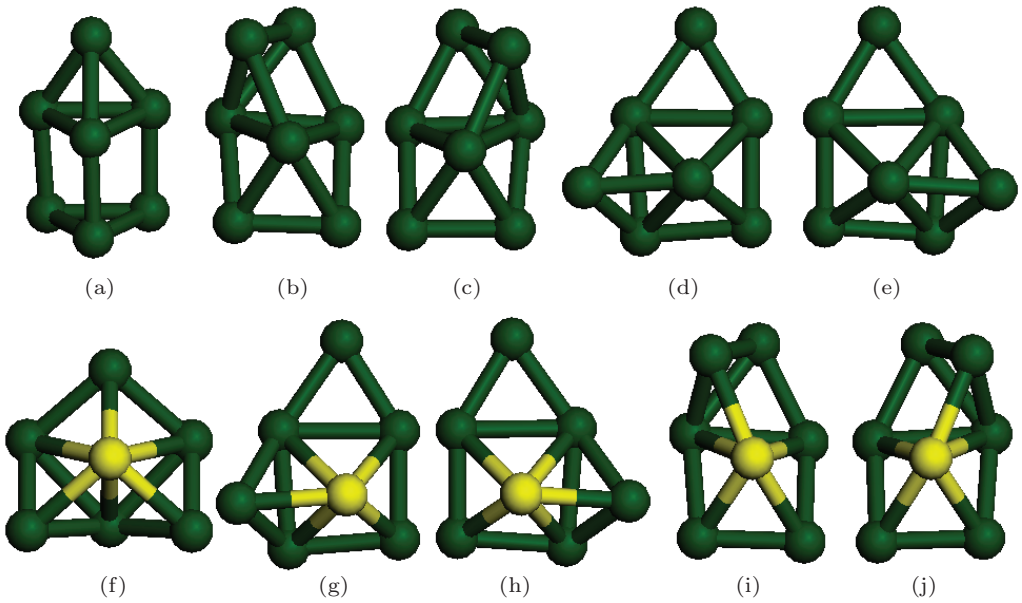


Fig. 1. (colour online) The lowest-energy structures and the equilibrium structures of the low-lying isomers for pure Pt_7 cluster and MPt_6 clusters. The M atom is represented by a flavicant sphere. Structures (a)–(j) are explained in detail in the text.

Table 1. Geometric structures (STRs), the symmetry types (SYMs), the spin multiplicities (SMs), and the energy separations of the isomeric structures from the ground-state structures (ΔE_s) of MPt_6 clusters.

Cluster	Ground state			Low-lying isomer							
	STR	SM	SYM	STR	SM	SYM	ΔE/eV	STR	SM	SYM	ΔE/eV
Pt_7	(a)	5	C_{3v}	(b), (c)	3	C_2	0.081	(d), (e)	5	C_1	0.407
$ScPt_6$	(f)	2	C_s	(g), (h)	2	C_1	0.075	(i), (j)	2	C_1	0.311
$TiPt_6$	(f)	1	C_s	(g), (h)	3	C_1	0.311	(i), (j)	3	C_1	0.348
VPt_6	(f)	2	C_1	(g), (h)	2	C_1	0.143	(i), (j)	6	C_1	0.345
$CrPt_6$	(f)	3	C_s	(g), (h)	3	C_1	0.128	(i), (j)	5	C_1	0.242
$MnPt_6$	(g), (h)	8	C_1	(f)	8	C_s	0.038	(i), (j)	8	C_1	0.131
$FePt_6$	(g), (h)	7	C_1	(f)	7	C_s	0.011	(i), (j)	9	C_1	0.131
$CoPt_6$	(g), (h)	6	C_1	(i), (j)	6	C_1	0.092	(f)	6	C_s	0.127
$NiPt_6$	(g), (j)	5	C_1	(f)	5	C_s	0.020	(g), (h)	5	C_1	0.027
$CuPt_6$	(g), (h)	4	C_1	(i), (j)	4	C_1	0.194	(f)	2	C_s	0.272
$ZnPt_6$	(g), (h)	3	C_1	(f)	3	C_s	0.190	(i), (j)	3	C_1	0.195

The ground state structure of Pt_7 is found to be a triangle-capped prism with C_{3v} symmetry (Fig. 1(a)), which has not been reported in the literature. Tian *et al.*[20] reported that the coupled tetragonal pyramid structure is of the ground state for Pt_7, which is 0.226 eV higher in energy than structure (a) in our calculations. The different assignments of the ground state structure may be due to the different calculation methods. Structures (b) and (c) are chiral structures, which are 0.081 eV higher in energy than the ground-state structure. The difference between structures (b) and (c) is the open end direction of the quadrangular-pyramid cap on the quadrangular pyramid. Structures (d) and (e) are also chiral structures. Each of them is edge- and triangle-capped on the quadrangular pyramid, the difference is the relative position of the triangle cap to the edge cap, one lies on the left, and the other lies on the right.

The ground state structures and some low-lying metastable isomers of MPt_6 (M= Sc, Ti, V, Cr, Mn, Fe, Co, Ni, Cu, and Zn) are shown in Fig. 1 (structures (f)–(j)). Our calculations show that structure (f) (C_s symmetry) is the ground-state structure of the MPt_6 clusters with M=Sc, Ti, V, and Cr (number of

d electrons in the M atoms is $n_{\rm d} = 1$–4), while structure (g) (or the chiral structure (h)) is the ground-state structure of the MPt$_6$ clusters with M=Mn, Fe, Co, Cu, and Zn ($n_{\rm d} = 5$–7 and 10). Structure (g) can be constructed by replacing an atom in structure (d) of the Pt$_7$ cluster. The ground-state structure of the NiPt$_6$ cluster ($n_{\rm d} = 8$) is structure (i) (or the chiral structure (j)), which can be constructed by replacing an atom in structure (b) of Pt$_7$. It is interesting to note that the three types of structures (including the chiral structures) of MPt$_6$ are all composed of a quadrangular pyramid moiety with the M atom as the vertice and two additional Pt atoms. The two Pt atoms are located on two three-fold hollow sites of the quadrangular pyramid moiety (structure (f)), or on one three-fold hollow site and one edge site (structures (g) and (h)), or on two edge sites of the same three-fold hollow (structures (i) and (j)). Structure (a) of Pt$_7$ has no quadrangular pyramid moiety and is not suitable for the doped clusters MPt$_6$. Zhang *et al.*[18] reported the structures and the stabilities of the MAu$_6$ (M=Sc, Ti, V, Cr, Mn, Fe, Co, Ni, Cu, and Zn) clusters and suggested that the partially filled d shell of the M atom plays a crucial role in determining the structure and the property of the corresponding MAu$_6$ cluster. However, in our calculations, the ground-state structures of the full 3d shell transition-metal doped clusters CuPt$_6$ and ZnPt$_6$ are similar to those of the open 3d shell transition-metal doped clusters MnPt$_6$/FePt$_6$/CoPt$_6$.

3.2. Relative stability

In this subsection, we discuss the relative stabilities of the MPt$_6$ clusters according to several physical quantities and the calculated results given in Table 2.

Table 2. Binding energies per atom, doping energies, HOMO–LUMO energy gaps, average Pt–Pt bond lengths, and average M–Pt bond lengths of the ground states of MPt$_6$.

Cluster	Structure	$E_{\rm b}$/eV	$E_{\rm d}$/eV	$E_{\rm gap}$/eV	$R_{\rm Pt-Pt}$/Å	$R_{M-{\rm Pt}}$/Å
Pt$_7$	(a)	3.695	–	0.389	2.545	–
ScPt$_6$	(f)	4.220	6.554	0.190	2.548	2.675
TiPt$_6$	(f)	4.287	7.025	0.658	2.578	2.522
VPt$_6$	(f)	3.997	5.992	0.491	2.576	2.495
CrPt$_6$	(f)	3.662	3.652	0.590	2.571	2.491
MnPt$_6$	(g), (h)	3.678	3.758	0.303	2.533	2.587
FePt$_6$	(g), (h)	3.987	5.925	0.371	2.547	2.483
CoPt$_6$	(g), (h)	3.871	5.115	0.272	2.532	2.511
NiPt$_6$	(i), (j)	4.632	7.440	0.316	2.541	2.469
CuPt$_6$	(g), (h)	3.472	2.324	0.192	2.517	2.587
ZnPt$_6$	(g), (h)	3.319	1.246	0.293	2.531	2.585

The binding energy per atom ($E_{\rm b}$) of the MPt$_6$ clusters is defined as $E_{\rm b} = [E(M) + 6E({\rm Pt}) - E(M{\rm Pt}_6)]/7$, where $E(M)$, E(Pt), and $E(M$Pt$_6)$ represent the binding energies of M, Pt, and MPt$_6$ cluster, respectively. The $E_{\rm b}$ of a given cluster is a measure of its thermodynamic stability. It can be seen that the $E_{\rm b}$ values of the MPt$_6$ clusters except for M = Cr, Mn, Cu, and Zn are higher than that for the pure Pt$_7$ cluster, indicating that these doped transition metal atoms can stabilize the doped clusters. The $E_{\rm b}$ of NiPt$_6$ is the largest and that of ZnPt$_6$ is the smallest, indicating that the former is the most stable and the latter is the least stable among the MPt$_6$ clusters.

For understanding the structural evolutions of the MPt$_6$ clusters from Pt$_6$, we also calculate the doping energy $E_{\rm d} = E(M) + E({\rm Pt}_6) - E(M{\rm Pt}_6)$, where E(Pt$_6$) is the binding energy of Pt$_6$. The lowest-energy structure of Pt$_6$ in our computational method is a nearly equilateral triangle, which is in accordance with the previous work.[17] It is clear that NiPt$_6$ has the highest doping energy, while ZnPt$_6$ has the lowest one.

To further analyze the stabilities of the MPt$_6$ clusters, the average bond lengths of Pt–Pt bonds ($R_{\rm Pt-Pt}$) and M–Pt bonds ($R_{M-{\rm Pt}}$) of the ground-state structures are also given in Table 2. The difference in $R_{\rm Pt-Pt}$ between Pt$_7$ and MPt$_6$ is very small (no more than 0.06 Å). However, the differences in $R_{M-{\rm Pt}}$ for different MPt$_6$ clusters are clear. The Ni–

Pt bond in $NiPt_6$ is the shortest, which is consistent with the fact that $NiPt_6$ has the highest E_b and E_d. The M–Pt bonds in $CuPt_6$ and $ZnPt_6$ are longer than those in most of the remaining MPt_6 clusters except for Sc and Mn, which is in accordance with the lowest E_b and E_d for $CuPt_6$ and $ZnPt_6$. Based on the analysis above, we may conclude that $NiPt_6$ is most stable, while $CuPt_6$ and $ZnPt_6$, which both have close d shells, are the least stable among the calculated MPt_6 clusters.

The energy gap between the highest occupied molecular orbital (HOMO) and the lowest unoccupied molecular orbital (LUMO), that is $E_{gap} = E_{LUMO} - E_{HOMO}$, of the MPt_6 cluster is listed in Table 2. The E_{gap} is an important quality to characterize the stability and the chemical activity of the cluster. A smaller energy gap indicates the easier transition of electron from HOMO to LUMO and the easier combination of the electron on the HOMO orbital with the other atoms to form chemical bonds. A large energy gap corresponds to a higher stability. In addition, the energy gap also determines the conductivity of the cluster, the smaller the energy gap, the stronger the electrical conductivity. As can be seen from Table 2, the E_{gap} values of MPt_6 show the jagged oscillation behavior. The E_{gap} values of the MPt_6 clusters with M=Sc, V, Mn, Co, and Cu, which each have odd number electrons, are much smaller than those of their neighbors. The E_{gap} values of $ScPt_6$ and $TiPt_6$ are the relative minimum and the relative maximum, respectively, which indicate that $ScPt_6$ has the highest chemical activity and the best conductivity, while $TiPt_6$ has the lowest chemical activity and the weakest conductivity. The E_{gap} of $CuPt_6$ is almost equal to that of $ScPt_6$, which suggests that the chemical activity of $CuPt_6$ is also high. Among all the MPt_6 clusters, only $TiPt_6$, VPt_6, and $CrPt_6$ have larger E_{gap} values than the pure Pt_7 cluster, which indicates that the three clusters are relatively more chemically stable than the neighboring clusters, while the doping of the other TM atoms may stabilize the Pt_7 clsuter.

3.3. Magnetic properties

The magnetic properties of the MPt_6 (M=Sc, Ti, V, Cr, Mn, Fe, Co, Ni, Cu, and Zn) clusters are also studied. The total magnetic moments and the spin populations on the M atoms of the MPt_6 clusters are shown in Table 3. All the clusters are magnetic except the $TiPt_6$ cluster, although the ground-state structure of $TiPt_6$ is similar to those of the MPt_6 (M=Sc, V, Cr) clusters. The magnetic moments of the MPt_6 clusters are 1 μ_B, 0 μ_B, 1 μ_B, 2 μ_B, 7 μ_B, 6 μ_B, 5 μ_B, 4 μ_B, 3 μ_B, and 2 μ_B for M=Sc, Ti, V, Cr, Mn, Fe, Co, Ni, Cu, and Zn, respectively. From $MnPt_6$ to $ZnPt_6$, the total magnetic moment decreases gradually from 7 μ_B to 2 μ_B following the gradual reduction of the number of unpaired d electrons. Since the magnetic moments of the MPt_6 clusters vary from 0 μ_B to 7 μ_B, we can confirm that doping different 3d transition metal into the Pt_6 cluster has the potential utility in designing new spintronic nanomaterials with tunable magnetic properties.

Table 3. Magnetic moments of the ground-state MPt_6 (M= Sc, Ti, V, Cr, Mn, Fe, Co, Ni, Cu, and Zn) clusters m, the Mulliken charge on the M atoms ρ_M, and the total and the partial (population on 3d, 4s, 4p orbitals) magnetic moments of the M atoms m_M. The magnetic moments are in units of μ_B, and the charge is in units of $|e|$.

Cluster	m	ρ_M	m_M	m_M(3d)	m_M(4s)	m_M(4p)
$ScPt_6$	1	1.077	–0.036	–0.026	–0.005	–0.004
$TiPt_6$	0	0.089	0.000	0.000	0.000	0.000
VPt_6	1	0.704	1.245	1.152	0.049	0.045
$CrPt_6$	2	0.646	2.551	2.375	0.076	0.104
$MnPt_6$	7	0.574	4.561	4.310	0.147	0.110
$FePt_6$	6	0.598	3.654	3.480	0.101	0.080
$CoPt_6$	5	0.430	2.346	2.259	0.055	0.037
$NiPt_6$	4	0.455	1.282	1.230	0.030	0.025
$CuPt_6$	3	0.300	0.062	0.089	–0.015	–0.012
$ZnPt_6$	2	0.410	0.007	–0.003	0.018	–0.007

To obtain a further insight into the magnetic nature of the MPt_6 clusters, we perform a detailed analysis of the Mulliken charge and the local magnetic moments on M and Pt atoms. For $ScPt_6$, $CuPt_6$, and $ZnPt_6$, the total magnetic moments (1 μ_B, 3 μ_B, and 2 μ_B) are located mainly on the Pt atoms (0.964 μ_B,

2.939 μ_B, and 1.993 μ_B). The local magnetic moments are aligned ferromagnetically for $CuPt_6$ and $ZnPt_6$, and antiferromagnetically for $ScPt_6$. For VPt_6 and $CrPt_6$, the total magnetic moments (1 μ_B and 2 μ_B) are located mainly on the M atoms (1.251 μ_B and 2.563 μ_B), and the local magnetic moments on the Pt atoms are both aligned ferromagnetically. For the MPt_6 (M=Mn, Fe, Co and Ni) clusters, all the clusters are aligned ferromagnetically, and the total magnetic moments (7 μ_B, 6 μ_B, 5 μ_B, and 4 μ_B) are located on both M (4.560 μ_B, 3.654 μ_B, 2.336 μ_B, and 1.259 μ_B) and Pt atoms. The magnetic moment of $TiPt_6$ is quenched (the local magnetic moments of M and Pt atoms are 0 μ_B).

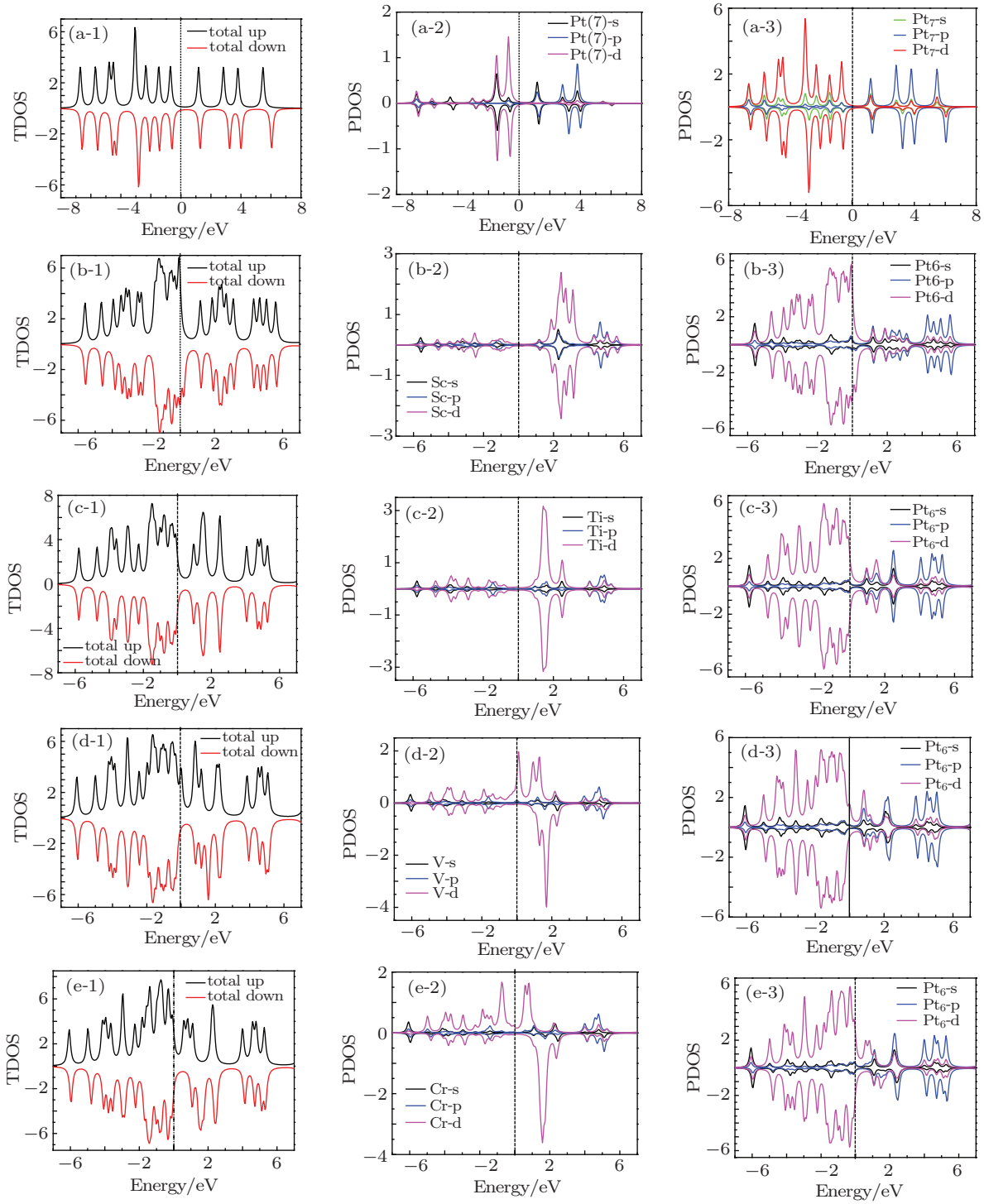


Fig. 2. (colour online) Total DOS (TDOS) and partial DOS (PDOS) of (a) Pt_7 and MPt_6 ((b) Sc, (c) Ti, (d) V, and (e) Cr) clusters. Spin up (positive) and spin down (negative) densities are given in each case. The dashed line indicates the location of the HOMO level.

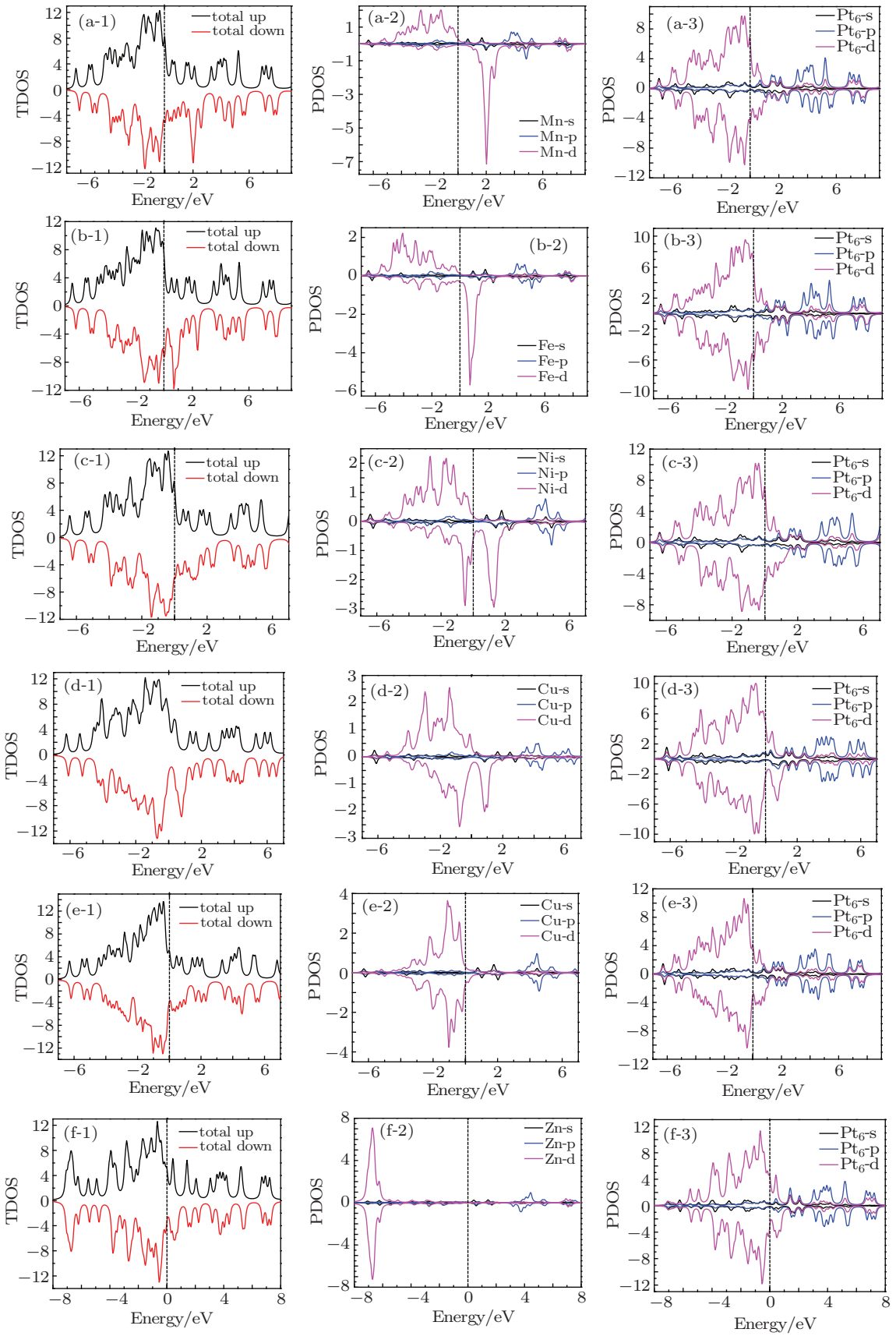


Fig. 3. (colour online) TDOS and PDOS of the $M\mathrm{Pt}_6$ ((a) Mn, (b) Fe, (c) Co, (d) Ni, (e) Cu, and (f) Zn) clusters. Spin up (positive) and spin down (negative) densities are given in each case. The dashed line indicates the location of the HOMO level.

To gain more information about the magnetic properties, we also perform the Mulliken population analysis for the lowest-energy structures and the atomic charge on the M atoms in the $M\mathrm{Pt}_6$ clusters, and the results are listed in Table 3. For all the clusters, the charge is transferred from the Pt atom to the M atom, which indicates that the 3d electrons of the transition metals play a dominant role in determining the magnetism of the $M\mathrm{Pt}_6$ clusters, whereas the s and the p electrons contribute only a little to the net spin for most of the $M\mathrm{Pt}_6$ clusters.

To explain the phenomenon of the magnetic moment in $M\mathrm{Pt}_6$, the total densities of state (TDOSs) and partial densities of state (PDOSs) are all calculated and shown in Figs. 2 and 3. The TDOS and PDOS of the Pt_7 cluster are also given in Fig. 2. The DOS is obtained by the Gaussian extension applied to the eigenvalues, and the broadening width parameter is chosen to be 0.1 eV. The Fermi level of cluster is presented as a dashed vertical line and shifted to zero. Spin-up (positive) and spin-down (negative) densities are given in each case. As shown in the two figures, in the vicinity of and below the Fermi level, all the electronic states come mainly from the 3d states in the transition metals and the 5d states in the Pt atoms of the $M\mathrm{Pt}_6$ clusters. In most cases, the two states have more or less d–d hybridization. However, over the Fermi level, the 6s and the 5p states of the Pt atom cannot be ignored compared with the 5d state, which generate the s–p–d hybridization in the $M\mathrm{Pt}_6$ clusters. For the six Pt atoms in the $M\mathrm{Pt}_6$ cluster, because of the hybridization with the transition metal atoms, their orbital energy levels become broadened compared with that of the pure Pt_7 cluster. Because of the hybridizations of atom orbits in the $M\mathrm{Pt}_6$ clusters, the magnetic moments of the 3d transition metal atoms are higher or lower than those obtained from the Hund's rule. Especially, the TiPt_6 cluster has no magnetic moment. Moreover, the magnetic moments of Pt atoms play an important role in determining the total magnetic moment of the corresponding $M\mathrm{Pt}_6$ cluster. We take the PDOSs of Sc and Pt_6 in the ScPt_6 cluster and those of Mn and Pt_6 in MnPt_6 as two examples. In ScPt_6 and MnPt_6, the valence electron configurations of the free atoms Sc and Mn are $3\mathrm{d}^1 4\mathrm{s}^2$ and $3\mathrm{d}^5 4\mathrm{s}^2$, respectively. According to the Hund's rule, the magnetic moments of Sc and Mn atoms are 1 μ_B and 5 μ_B, respectively. As Sc and Mn are doped into the Pt_6 cluster, because of the hybridization between the atomic orbits of the guest and the host atoms, the magnetic moments of Sc and Mn atoms reduce to -0.036 μ_B and 4.560 μ_B, respectively, although the total magnetic moments of ScPt_6 and MnPt_6 are still 1 μ_B and 7 μ_B, respectively. As both the Cu and the Zn atoms have full filled d shells, the TDOSs and the PDOSs of CuPt_6 and ZnPt_6 shown in Fig. 3 have some differences from those of the other clusters, although their structures are similar. The 3d spin-up and spin-down states of Cu and Zn are so matched that they can be regard to have no contribution to their total magnetic moments of the clusters. The total magnetic moments of CuPt_6 and ZnPt_6 are 3 μ_B and 2 μ_B, respectively, which come mainly from the contribution of the Pt atoms.

4. Conclusion

In the present study, the structural, electronic, and magnetic properties of the transition metal doped Pt_6 clusters are studied using the relativistic all-electron density functional theory with the generalized gradient approximation. The calculated results show that all the ground states of the $M\mathrm{Pt}_6$ clusters have similar structures, which can be regarded as some-capped quadrangular pyramids. Most of the doped structures show larger binding energies than the pure Pt_7 cluster, indicating that doping the transition metal atoms can stabilize the pure platinum cluster. The HOMO–LUMO gap results show that most of the doped clusters have higher chemical activities than the pure Pt_7 cluster. The magnetism calculations demonstrate that the variation range of the magnetic moments of the $M\mathrm{Pt}_6$ clusters is from 0 μ_B to 7 μ_B, indicating that the $M\mathrm{Pt}_6$ clusters can have the potential utility in designing new spintronic nanomaterials with tunable magnetic properties.

Acknowledgment

We thank Prof. Yang Jin-Long for his helpful discussion. All the computations were carried out at the supercomputer center of University of Science and Technology of China.

References

[1] Bashyam R and Zelenay P 2006 *Nature* **443** 63
[2] Gasteiger H A and Nenad M 2009 *Science* **324** 48
[3] Zhang J J, Bing Y H, Liu H S, Zhang L and Ghosh D 2010 *Chem. Soc. Rev.* **39** 2184

[4] Mun B S, Watanabe M, Rossi M, Stamenkovic V, Markovic N M and Ross J 2005 *J. Chem. Phys.* **123** 204717
[5] Lee Y S, Rhee J Y, Whang C N and Lee Y P 2003 *Phys. Rev.* B **68** 235111
[6] Toda T, Igarashi H, Uchida H and Watanabe M 1999 *J. Electrochem. Soc.* **146** 3750
[7] Antolini E, Passos R R and Ticianelli E A 2002 *Electrochim. Acta* **48** 263
[8] Xiong L and Manthiram A 2004 *Electrochim. Acta* **49** 4163
[9] Yano H, Kataoka M, Yamashita H, Uchida H and Watanabe M 2007 *Langmuir* **23** 6438
[10] Koh S, Leisch J, Toney M F and Strasser P 2007 *J. Phys. Chem.* C **111** 3744
[11] Stamenkovic V, Mun B S, Mayrhofer K J J, Ross P N, Markovic N M, Rossmeisl J, Greeley J and Nøskov J K 2006 *Angew. Chem. Int. Ed.* **45** 2897
[12] Nøskov J K, Rossmeisl J, Logadottir A, Lindqvist L, Kitchin J R, Bligaard T and Jónsson H 2004 *J. Phys. Chem.* B **108** 17886
[13] Yao C F, Zhuang L, Cao Y L, Ai X P and Yang H X 2008 *Int. J. Hydrogen Energy* **33** 2462
[14] Antolini E, Salgado J R C and Gonzalez E R 2006 *J. Power Sources* **160** 957
[15] Xiong L and Manthiram A 2005 *J. Electrochem. Soc.* **152** A697
[16] Xiong L and Manthiram A 2004 *J. Mater. Chem.* **14** 1454
[17] Wang M, Huang X W, Du Z L and Li Y C 2009 *Chem. Phys. Lett.* **480** 258
[18] Zhang M, He L M, Zhao L X, Feng X J and Luo Y H 2009 *J. Phys. Chem.* C **113** 6491
[19] Nie A H, Wu J P, Zhou C G, Yao S J, Luo C, Forrey R C and Cheng H S 2007 *Int. J. Quan. Chem.* **107** 219
[20] Tian W Q, Ge M F, Sahu B R, Wang D X, Yamada T and Mashiko S 2004 *J. Phys. Chem.* A **108** 3086
[21] Ordejón P, Artacho E and Soler J M 1996 *Phys. Rev.* B **53** R10441
[22] Sánchez-Portal D, Ordejón P, Artacho E and Soler J M 1997 *Int. J. Quantum. Chem.* **65** 453
[23] Delley B 1990 *J. Chem. Phys.* **92** 508
[24] Perdew J P and Wang Y 1992 *Phys. Rev.* B **45** 13244
[25] Pulay P 1980 *Chem. Phys. Lett.* **73** 393
[26] Airola M B and Morse M D 2002 *J. Chem. Phys.* **116** 1313
[27] Fabbi J C, Langenberg J D, Costello Q D, Morse M D and Karlsson L 2001 *J. Chem. Phys.* **115** 7543
[28] Taylor S, Lemire G W, Hamrick Y M, Fu Z and Morse M D 1988 *J. Chem. Phys.* **89** 5517